molecular pharmaceutics

Article

pubs.acs.org/molecularpharmaceutics

Pycup—A Bifunctional, Cage-like Ligand for ^{64}Cu Radiolabeling

Eszter Boros,*[,†] Elena Rybak-Akimova,[‡] Jason P. Holland,[§,∥] Tyson Rietz,[†] Nicholas Rotile,[†] Francesco Blasi,[†] Helen Day,[†] Reza Latifi,[‡] and Peter Caravan*[,†]

[†]The Athinoula A. Martinos Center for Biomedical Imaging, Department of Radiology, Massachusetts General Hospital, Harvard Medical School, 149 Thirteenth Street, Suite 2301, Charlestown, Massachusetts 02129, United States

[‡]Department of Chemistry, Tufts University, 62 Talbot Avenue, Medford, Massachusetts 02155, United States

[§]Division of Nuclear Medicine and Molecular Imaging, Massachusetts General Hospital, Department of Radiology, Harvard Medical School, 55 Fruit Street, White 427, Boston, Massachusetts 02114, United States

[∥]Life Sciences, Australian Nuclear Science and Technology Organisation, Kirrawee, New South Wales, 2232, Australia

Supporting Information

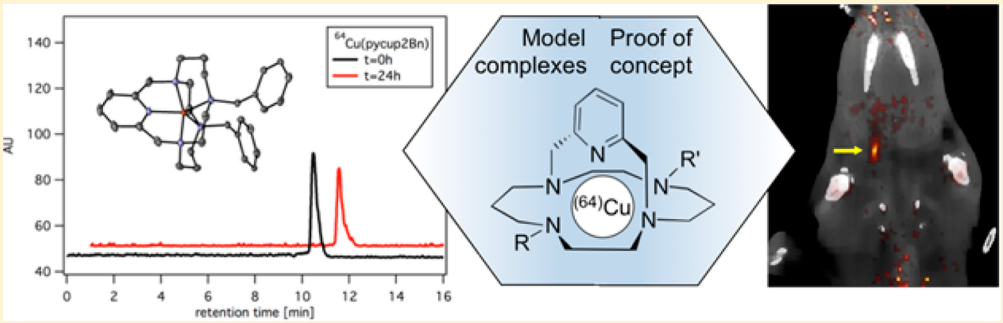

ABSTRACT: In developing targeted probes for positron emission tomography (PET) based on ^{64}Cu, stable complexation of the radiometal is key, and a flexible handle for bioconjugation is highly advantageous. Here, we present the synthesis and characterization of the chelator pycup and four derivatives. Pycup is a cross-bridged cyclam derivative with a pyridyl donor atom integrated into the cross-bridge resulting in a pentadentate ligand. The pycup platform provides kinetic inertness toward ^{64}Cu dechelation and offers versatile bioconjugation chemistry. We varied the number and type of additional donor atoms by alkylation of the remaining two secondary amines, providing three model ligands, pycup2A, pycup1A1Bn, and pycup2Bn, in 3−4 synthetic steps from cyclam. All model copper complexes displayed very slow decomplexation in 5 M HCl and 90 °C ($t_{1/2}$: 1.5 h for pycup1A1Bn, 2.7 h for pycup2A, 20.3 h for pycup2Bn). The single crystal crystal X-ray structure of the $[Cu(pycup2Bn)]^{2+}$ complex showed that the copper was coordinated in a trigonal, bipyramidal manner. The corresponding radiochemical complexes were at least 94% stable in rat plasma after 24 h. Biodistribution studies conducted in Balb/c mice at 2 h postinjection of ^{64}Cu labeled pycup2A revealed low residual activity in kidney, liver, and blood pool with predominantly renal clearance observed. Pycup2A was readily conjugated to a fibrin-targeted peptide and labeled with ^{64}Cu for successful PET imaging of arterial thrombosis in a rat model, demonstrating the utility of our new chelator *in vivo*.

KEYWORDS: *chelator, copper, positron emission tomography, fibrin*

INTRODUCTION

With the increased availability of cyclotrons capable of producing radiometals, the application of copper radionuclides for medical imaging has gained great interest.[1] In recent years, the long-lived isotope ^{64}Cu (β^+ 17.4%, E_{max} = 0.656 MeV, β^- 39%, E_{max} = 0.573 MeV) has received the greatest attention for this purpose.[2] Copper-64 has near ideal emission properties for positron emission tomography (PET); the β^+ is low energy which facilitates acquisition of high-resolution PET images.[3]

The longer half-life ($t_{1/2}$ = 12.7 h), compared to commonly used, but short-lived radionuclides ^{18}F, ^{11}C, or even ^{68}Ga is more applicable to developing targeted PET agents conjugated to larger biomolecules, such as peptides, antibodies, and antibody fragments that may require long circulation times before achieving optimal target uptake. The longer half-life also allows for remote production and shipment of the radionuclide over large distances and makes this radionuclide attractive for clinical application in PET. Several radiotracers based on ^{64}Cu are currently being evaluated in multicenter clinical trials.[4]

To utilize ^{64}Cu for targeted imaging, stable complexation of the metal to the targeting vector is key. Macrocyclic and cage-like hexadentate ligand systems are among the current front runners for stable coordination with minimal metal ion loss even after multiple days of incubation under physiologically

Received: November 13, 2013
Accepted: December 2, 2013
Published: December 2, 2013

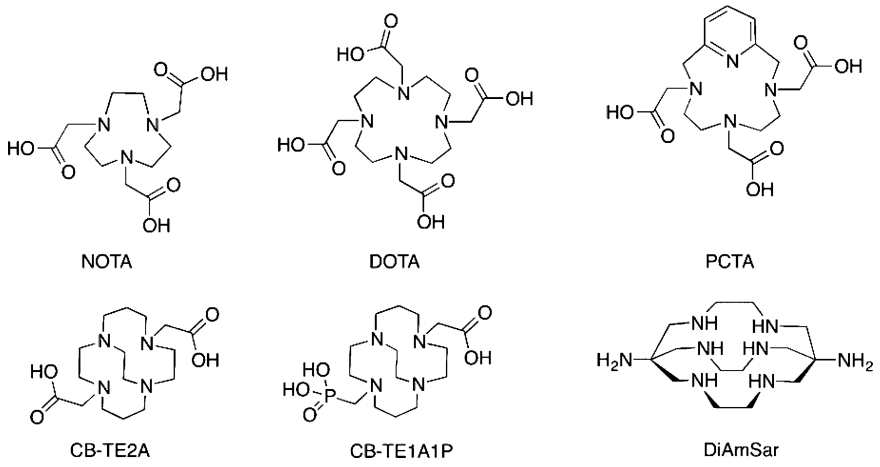

Figure 1. Structures of various chelators used for labeling with ^{64}Cu.

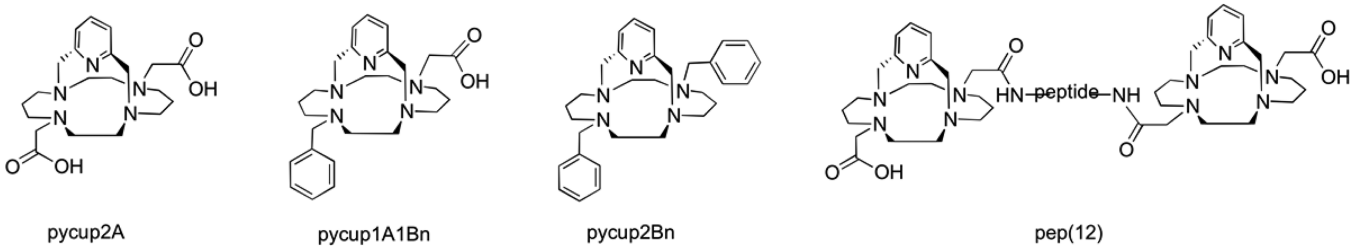

Figure 2. Structures of chelates investigated in this study (from left to right): pycup2A, pycup1A1Bn, pycup2Bn, and the peptide conjugate pep(12).

relevant conditions.[3] Acyclic chelates often fall victim to rapid decomplexation kinetics, resulting in the loss of the radiometal ion, characterized *in vivo* by persistent uptake of the Cu radionuclide in the liver and bound to plasma proteins.[5−7] It is important to note that 1,4,7,10-tetraazacyclododecane-1,4,7,10-tetraacetic acid (DOTA; Figure 1), often considered the workhorse ligand for radiometal-based nuclear medicine, has been well-documented to lack sufficient kinetic inertness for use as a ligand for Cu(II).[8,9] The ligands CB-TE2A, CB-TE1A1P, SarAr, and PCTA (3,6,9,15-tetraazabicyclo[9.3.1]-pentadeca-1(15),11,13-triene-3,6,9-triacetic acid; Figure 1) have proven to be more suitable for the formation of kinetically inert copper complexes.[10−16] NOTA (1,4,7-triazacyclononane-1,4,7-triacetic acid) can also provide an alternative in some cases.[17] While the kinetically inert complexation of ^{64}Cu is one requirement for a ^{64}Cu radiopharmaceutical, the charge, lipophilicity, and conjugation linker will each affect the behavior of the radiolabeled bioconjugates *in vivo*, often in an unpredictable manner.[11,16,18,19] Therefore, it is crucial to have an armamentarium of bifunctional chelators available. It was our goal to develop a new bifunctional chelator which would not only provide another alternative in the chelate tool-box, but also overcome various shortcomings of the currently available systems. Key requirements include: (1) facile chemical synthesis; (2) ease of ligand modification to alter overall charge; (3) slow decomplexation of the copper complex under forcing conditions; (4) rapid radiolabeling; (5) high kinetic inertness of the ^{64}Cu complex with respect to transchelation; and (6) bioconjugation and applicability to a target-specific peptide.

Inspired by the variety of macrocyclic ligand scaffolds, we designed a new ligand to have the capability to fulfill all criteria listed above. Recently published work on new Cu(II) chelators has shown that highly inert Cu-complexes can be obtained by modification of CB-TE2A-type structures, either by extension of the cross-bridge[20] or integration of a donor atom into the cross bridge.[21] We also took the potent copper chelator cyclam as a base and used the previously established synthesis of 1,8-(2,6-pyridinedimethylene)-1,4,8,11-tetraazacyclotetradecane (here abbreviated as pycup) by Brandes et al.[22] to furnish a ligand that incorporates a pyridyl nitrogen donor atom into the cross-bridge. Incorporation of this donor group for the purpose of building a more sturdy ligand is based on the well-documented preference of Cu(II) for softer nitrogen donors.[23−25]

To our knowledge, while similar ligands have been evaluated and found to be very inert chelators for Cu(II), the pycup structure or synthesis of potential pycup derivatives have not been further explored for this purpose. Closely related bis-amido-derivatives have been explored for the purpose of formation of multinuclear complexes in organic solvents.[26−28] For our purpose, we hoped that incorporation of a donor ligand into the cross-bridge would reduce the need for additional pendant arm donor atoms for stable coordination. The pendant arms can then be used as handles for bioconjugation, providing a versatile, easily synthesized chelator. To understand the impact of the number of donor atoms on coordination, we used the two residual secondary amines on the pycup ligand to introduce 0, 1, or 2 acetate arms as additional donors and charge equilibrators (pycup2A, pycup1A1Bn, and pycup2Bn, Figure 2). The corresponding copper complexes were used to study acid stability, labeling properties, and the inertness of the corresponding radiochemical complexes.

^{64}Cu-complexes have been used for the imaging of a number of protein targeting vectors, such as somatostatin analogues,[29−31] bombesin derivatives,[10,16,32] and RGD peptides.[11,17,33] We demonstrated that pycup2A could be used as a bifunctional ligand by conjugating it to a known fibrin-

dx.doi.org/10.1021/mp400686z | *Mol. Pharmaceutics* 2014, 11, 617−629

targeting peptide.[34] This conjugate was radiolabeled and subjected to the same kinetic inertness challenges as the model compounds, followed by its evaluation as a PET probe for thrombus imaging in a rat model.

EXPERIMENTAL SECTION

General Methods and Materials. ^{1}H and ^{13}C NMR spectra were recorded on a Varian 500 NMR system. Chemicals were supplied by Aldrich Chemical Co., Inc., and were used without further purification. Solvents (HPLC grade) were purchased from various commercial suppliers and used as received. Cyclam was received from Alfa Aesar (Ward Hill, MA, USA). 2,6-Bis(bromomethyl)pyridine was purchased from Sigma Aldrich, USA. Electronic spectra were recorded between 360 and 900 nm in 10 nm intervals on a Spectra max M2 (Molecular devices), using the SoftMax Pro software. Purification via high-performance liquid chromatography (HPLC) of intermediates was performed using HPLC methods A and B after injection of the filtered, crude mixture onto preparative HPLC (Rainin, Dynamax, column: 250 mm Phenomenex C18). Method A: mobile phase A = 50 mM ammonium acetate in water; mobile phase B = 10% 50 mM ammonium acetate in water, 90% MeCN; flow-rate 15 mL/min, 0−1 min: 5% B, 1−3 min: 5−40% B, 3−15 min: 40−80% B, 15−16 min: 80−95% B, 16−20 min: 95% B, 20−21 min: 95−5% B, 21−23 min: 5% B. Purification of the ligand−peptide conjugate FBP12 was done using method B: Mobile phase A = 0.1% trifluoroacetic acid in H_2O; mobile phase B = 0.1% trifluoroacetic acid in MeCN, flow rate 15−18 mL/min, 0−4 min: 5% B, 4−33 min: 5−40% B, 33−37 min: 40−95% B, 37−42 min: 95% B, 42−43 min: 95−5% B, 45−48 min: 5% B. HPLC purity analysis (both UV and MS detection) was carried out on an Agilent 1100 system (column: Phenomenex Luna, C18(2) 100/2 mm) with UV detection at 220, 254, and 280 nm by using method C: A gradient of A (10 mM ammonium acetate in water) to 95% B (50 mM ammonium acetate in water, 90% MeCN), flow rate 0.8 mL/min. 0−1 min: 5% B, 1−10 min: 5−95% B, 10−12 min: 95% B, 12−12.5 min: 95−5% B, 12.5−15 min: 5% B. Determination of radiochemical yield and purity was measured using method D using an Agilent 1100 Series HPLC unit with a Carroll/Ramsey radiation detector with a silicon PIN photodiode (column for reaction control and DOTA challenge: Phenomenex Luna 5u C18(2), 150 mm × 4.6 mm × 5 μm; column for plasma stability and blood draw analysis: Polaris C18 A 150 mm × 4.6 mm × 5 μm). Mobile phase A was 0.1% trifluoroacetic acid in H_2O and mobile phase B 0.1% trifluoroacetic acid in MeCN, flow rate 0.8 mL/min. 0−1 min: 5% B, 1−10 min: 5−95% B. 10−12 min: 95% B, 12−12.5 min 95−5% B, 15 min: 5% B.

1,8-(2,6-Pyridinedimethylene)-1,4,8,11-tetraazacyclotetradecane (pycup). The high dilution intramolecular dialkylation of cyclam with 2,6-bis(bromomethyl)pyridine was conducted as previously reported in literature by Brandes et al.[22] The product (0.22 g, 0.73 mmol) was afforded in a 14% yield starting from cyclam (1 g, 5 mmol). ^{1}H NMR (CD_3OD, 400 MHz, ppm): 7.83 (m, 1H), 7.28 (d, 2H), 4.15 (d, 2H), 3.82 (d, 2H), 3.31−2.84 (m, 16H), 2.62 (m, 2H), 2.07 (m, 2H). ^{13}C NMR (CD_3OD, 100 MHz, ppm): 156.8, 138.9, 121.0, 55.8, 54.3, 52.2, 48.7, 23.1. LC-ESI-MS: calcd for $C_{17}H_{30}N_5$: 304.4. Found: 304.4 $[M + H]^+$, R_t = 0.5 min (method C).

1,8-(2,6-Pyridinedimethylene)-2,4- (tert-butyldiacetato)-1,4,8,11-tetraazacyclotetradecane (pycup2A^{t}Bu). 1,8-(2,6-Pyridinedimethylene)-1,4,8,11-tetraazacyclotetradecane (0.102 g, 0.33 mmol) was dissolved in MeCN (10 mL). K_2CO_3 (10 equiv, 0.45 g, 3.3 mmol). *tert*-Butyl-bromoacetate (1.5 equiv, 0.098 g, 0.074 μL, 0.51 mmol) was added to the mixture, and the reaction was stirred at room temperature overnight. The mixture was then filtered, and the filtrate was reduced and purified using preparative HPLC (method A). The desired product eluted at 17.7 min. All fractions containing the pure product were pooled, and the organic solvent was removed by rotary evaporation. The aqueous residue was lyophilized to afford the product (0.04 g, 0.075 mmol, yield: 22%) as a colorless oil. Using this method, no monoalkylated product was isolated. ^{1}H NMR ($CDCl_3$, 500 MHz, ppm): 8.02 (m, 1H), 7.5 (m, 2H), 4.23−2.97 (m, 24H), 2.05−1.92 (m, 4H), 1.43 (s, 18H). ^{13}C NMR ($CDCl_3$, 125 MHz, ppm): 165.7, 160.8, 123.23, 119.4, 84.1, 56.6, 53.9, 52.3, 27.8, 20.4, 19.8. LC-ESI-MS: calcd for $C_{29}H_{50}N_5O_4$: 532.4. Found: 532.3 $[M + H]^+$, R_t = 7.1 min (method C).

1,8-(2,6-Pyridinedimethylene)-1,4,8,11-tetraazacyclotetradecane-2,4-diacetic Acid (pycup2A). 1,8-(2,6-Pyridinedimethylene)-2,4- (*tert*-butyldiacetato)-1,4,8,11-tetraazacyclotetradecane (0.04 g, 0.075 mmol) was dissolved in a 1:1 mixture of dichloromethane and trifluoroacetic acid (3 mL). The reaction mixture was stirred overnight at room temperature. The solvent was removed *in vacuo*, and the oily residue was brought up a minimal amount of H_2O and lyophilized to afford the product as a white solid (0.045 g, 0.075 mmol, quantitative yield, with product as di-TFA salt). ^{1}H NMR (CD_3OD, 500 MHz, ppm): 8.15 (s, br, 1H), 7.62 (s, br, 2H), 4.90−3.97 (m, 4H), 3.87−1.85 (m, 20H). ^{13}C NMR (CD_3OD, 125 MHz, ppm): 171.9, 159.8, 140.7, 122.9, 55.2, 53.8, 53.2, 53.0, 52.8, 52.5, 51.6, 51.2, 50.2, 49.1, 48.2, 46.4, 44.6, 19.2. LC-ESI-MS: calcd for $C_{21}H_{34}N_5O_4$: 420.3. Found: 420.3 $[M + H]^+$, R_t = 1.1 min (method C).

1,8-(2,6-Pyridinedimethylene)-4-benzyl-1,4,8,11-tetraazacyclotetradecane (pycup1Bn). 1,8-(2,6-Pyridinedimethylene)-1,4,8,11-tetraazacyclotetradecane (0.187g, 0.61 mmol) was dissolved in MeCN (20 mL). K_2CO_3 (0.18 g, 1.3 mmol) and benzylbromide (0.068 g, 0.047 mL, 0.4 mmol) were added to the solution, and the reaction mixture was stirred at room temperature overnight. Subsequently, the solid components were filtered off, and the solvent was partially removed *in vacuo*. The residue was then purified using preparative HPLC (method A). The desired product eluted at 8.6 min. All fractions containing the pure product were pooled, and the organic solvent was removed by rotary evaporation. The aqueous residue was lyophilized to afford the product (0.131 g, 0.35 mmol, yield: 55%) as a yellow semisolid. ^{1}H NMR (CD_3OD, 400 MHz, ppm): 7.74 (m, 1H), 7.36 (m, 5H), 7.20 (d, 2H), 4.03 (d, 1H), 4.02 (s, 2H), 3.98 (d, 1H), 3.45 (dd, 2H), 3.21−2.37 (m, 18H), 1.72 (m, 2H). ^{13}C NMR (CD_3OD, 100 MHz, ppm): 159.6, 157.8, 137.9, 139.3, 128.3, 127.9, 121.0, 120.2, 138.9, 121.0, 58.8, 57.9, 53.7, 52.8, 52.1, 52.0, 48.8, 24.8, 24.2. LC-ESI-MS: calcd for $C_{24}H_{36}N_5$: 394.3. Found: 394.3 $[M + H]^+$, R_t = 5.6 min (method C).

1,8-(2,6-Pyridinedimethylene)-2,4-dibenzyl-1,4,8,11-tetraazacyclotetradecane (pycup2Bn). 1,8-(2,6-Pyridinedimethylene)-2,4-dibenzyl-1,4,8,11-tetraazacyclotetradecane was isolated from the reaction for the formation of 1,8-(2,6-pyridinedimethylene)-4-benzyl-1,4,8,11-tetraazacyclotetradecane as a side product but can be selectively synthesized by alkylation with 2 equivalents of benzyl bromide. The product was purified using preparative HPLC (method A). The desired product eluted at 18 min. All fractions containing the pure

dx.doi.org/10.1021/mp400686z | *Mol. Pharmaceutics* 2014, 11, 617−629

product were pooled, and the organic solvent was removed by rotary evaporation. ^{1}H NMR (CD_3OD, 400 MHz, ppm): 7.38−7.28 (m, 13H), 4.11−3.52 (m, 12H), 2.99−2.72 (m, 16H). ^{13}C NMR (CD_3OD, 100 MHz, ppm): 159.3, 138.2, 130.8, 128.7, 128.5, 121.1, 58.2, 53.4, 53.3, 22.3. LC-ESI-MS: calcd for $C_{31}H_{42}N_5$: 484.3. Found: 484.4 $[M + H]^+$, R_t = 8.7 min (method C).

1,8-(2,6-Pyridinedimethylene)-4-benzyl-8-(tert-butylacetato)-1,4,8,11-tetraazacyclotetradecane (pycup1A^{t}BuBn). 1,8-(2,6-Pyridinedimethylene)-4-benzyl-1,4,8,11-tetraaza-cyclotetradecane (0.032 g, 0.081 mmol) was dissolved in a 1:3 mixture of DMF and MeCN (4 mL) and heated to 50 °C. K_2CO_3 (0.1 g, 0.72 mmol) and KI (0.1 g, 0.6 mmol) were added to the solution, followed by a portion-wise addition of *tert*-butyl-bromoacetate (2.5 equiv, 0.03 mL, 0.039 g, 0.2 mmol) every 24 h (0.01 mL portions). After 72 h, no starting material was detected by LCMS. The solution was diluted with H_2O (1 mL), and the reaction mixture was filtered and purified with preparative HPLC (modified method A, with hold of 95% B solvent for 7 min instead of 4). The desired product elutes with a retention time of 17 min. The corresponding fractions were pooled, and the MeCN portion of the solvent was removed by rotary evaporation. The residual solvent was removed by lyopohilization to afford the product as a light yellow semisolid (0.013 g, 0.025 mmol, yield: 31%). ^{1}H NMR (CD_3OD, 500 MHz, ppm): 7.83 (m, 1H), 7.45−7.22 (m, 7H), 4.32−3.95 (m, 6H), 3.46−2.33 (m, 20H), 1.51 (m, 1H), 1.47 (s, 9H), 1.28 (m, 1H). ^{13}C NMR (CD_3OD, 125 MHz, ppm): 170.5, 138.6, 131.7, 129.4, 129.3, 128.7, 127.4, 121.9, 120.3, 80.9, 59.9, 57.3, 55.6, 53.9, 53.2, 53.1, 52.9, 51.9, 49.8, 49.4, 47.1, 26.3, 21.5. LC-ESI-MS: calcd for $C_{30}H_{46}N_5O_2$: 508.4. Found: 508.4 $[M + H]^+$, R_t = 6.1 min (method C).

1,8-(2,6-Pyridinedimethylene)-4-benzyl-1,4,8,11-tetraaza-cyclotetradecane-8-acetic acid (pycup1A1Bn). 1,8-(2,6-Pyridinedimethylene)-4-benzyl-8-(*tert*-butyl-acetato)-1,4,8,11-tetraazacyclotetradecane (0.003 g, 6 μmol) was dissolved in a 1:1 mixture of dichloromethane and trifluoroacetic acid (3 mL). The reaction mixture was stirred overnight at room temperature. The solvent was removed *in vacuo*, and the oily residue was brought up a minimal amount of H_2O and lyophilized to afford the product as a white solid (0.002 g, 5.9 μmol, quantitative yield, with product as the nTFA salt). ^{1}H NMR (CD_3OD, 400 MHz, ppm): 7.91 (m, 1H), 7.65−7.21 (m, 7H), 4.81−1.72 (m, 28H). ^{13}C NMR (CD_3OD, 125 MHz, ppm): 178.1, 160.6, 160.2, 131.7, 131.1, 130.1, 129.1, 128.8, 121.8, 58.1, 54.3, 52.9, 52.5, 50.9, 21.0. LC-ESI-MS: calcd for $C_{26}H_{38}N_5O_2$: 452.3. Found: 452.3 $[M + H]^+$, R_t = 3.2 min (method C).

pep(12). pycup2A·2TFA (0.015 g, 0.03 mmol) and PyBOP (benzotriazol-1-yl-oxytripyrrolidinophosphonium hexafluorophosphate, 0.014 g, 0.035 mmol) were dissolved in DMF (dimethylformamide, 1 mL). DIPEA (*N*,*N*-diisopropylethylamine) was added in 2 μL aliquots in order to adjust the pH of the solution to 7. After 5 min, Pep2 (0.012 g, 0.008 mmol, synthesized using standard solid phase methods; sequence H-[Phe-His-Cys-Hyp-Tyr(3-Cl)-Asp-Leu-Cys-His-Ile-Gln cyclic (2 → 8) disulfide]-1-(4-(aminomethyl)benzyl) acetamide) was dissolved in DMF and added dropwise to the preactivated ligand solution. Subsequently, the pH of the reaction mixture was readjusted to 7 using additional 2 μL aliquots of DIPEA. The reaction was then allowed to stir overnight at room temperature. After 24 h, the crude reaction mixture was analyzed using LCMS and was found to contain product, while all starting materials had been consumed and only trace amounts of ligand−peptide conjugates containing only one chelate were observed. The product was isolated using preparative HPLC (method B), eluting at 24.1 min. The corresponding fractions containing pure product were collected, and the solvent was removed *in vacuo* to afford the product as a white powder (0.002 g, 0.8 μmol, 10% purified yield). LC-ESI-MS: calcd for $C_{113}H_{160}ClN_{27}O_{21}S_2$: 2331.1. Found: 1165.1 $[M + 2H]^{2+}$. R_t = 4.5 min (method D).

Nonradioactive Copper Complexes. The general procedure was as follows: Ligand (0.04 mmol) was dissolved in MeOH (1 mL). $Cu(ClO_4)_2·6H_2O$ (0.04 mmol) was dissolved in MeOH (1 mL) and added dropwise to the ligand solution. The ligand was subsequently deprotonated using 2 equiv of NaOH (1 M aqueous solution). Upon addition of the base, a stark change of color from light to dark blue/green was observed. Solid components of the complexation reaction were removed using a 0.2 μm filter. The filtrate was collected and purified using solid phase extraction (C18 sep pak). The fractions containing the product were collected, and the solvent was removed *in vacuo* to afford the desired copper complex as a blue ($[Cu(pycup2Bn)][ClO_4]_2$), turquoise ([Cu-(pycup1A1Bn)]), or green powder ($[Cu(pycup2Bn)][ClO_4]$). All complexes were analyzed for purity using LC-MS, method C. Na[Cu(pycup2A)] LC-ESI-MS: calcd for $C_{21}H_{34}CuN_5O_4$: 482.18. Found: 482.2 $[M + 2H]^+$, R_t = 1.5 min. UV−vis: λ_{max} = 710 nm, ε = 116 M^{-1} cm^{-1}. [Cu(pycup1A1Bn)] LC-ESI-MS: calcd for $C_{26}H_{36}CuN_5O_2$: 513.22. Found: 513.2 $[M]^+$, R_t = 7.1 min. UV−vis: λ_{max} = 680 nm, ε = 133 M^{-1} cm^{-1}. $[Cu(pycup2Bn)][ClO_4]_2$ LC-ESI-MS: calcd for $C_{31}H_{41}ClCuN_5$: 581.23. Found: 581.2 $[M + Cl^-]^+$, R_t = 7.0 min. UV−vis: λ_{max} = 670 nm, ε = 268 M^{-1} cm^{-1}. $[Cu(FBP12)][ClO_4]_2$ LC-ESI-MS: Found: 581.2 $[M + 2H]^{2+}$, R_t = 4.5 min.

X-ray Crystallography and Structural Refinement Details. A blue plate crystal of the macrocyclic copper(II) complex was mounted on the Mitogen mount using paraton oil. X-ray intensity data were measured at 100 K with a Bruker D8 Quest diffractometer (equipped with a Photon CMOS detector and a Triumph monochromator) using Mo Kα radiation (λ = 0.71073 Å). The raw data frames were integrated with the SAINT+ program; corrections for Lorenz and polarization effects were applied. An empirical absorption correction based on multiple measurements of equivalent reflections was applied using the program SADABS. The structure was solved by the intrinsic phasing method (SHELX 2013)[35] and refined by full-matrix least-squares on F^2 with SHELXL.[36] All non-hydrogen atoms (except for disordered solvent) were refined anisotropically; hydrogens were placed in calculated positions. Benzyl groups of the macrocycle and chloride counterions were refined as disordered. Sheets of macrocyclic cations are separated by layers filled with disordered solvent molecules (which were not individually modeled, but rather collectively taken into account using the SQUEEZE module of Platon) and chloride counterions; the overall stoichiometry (3Cl:Cu) suggests a singly protonated species must be present in the solvent. Crystallographic information is available in the cif. Note: Atom numbering in cif differs from given numbering in manuscript.

Computational Details. All calculations were conducted using density functional theory (DFT) as implemented in the Gaussian03W suite of *ab initio* quantum chemistry programs.[37] Geometry optimizations and vibrational frequency calculations were performed by using the unrestricted B3LYP exchange and

correlation functionals and the double-ζ LANL2DZ basis set for all atoms.[38,39] Normal self-consistent field (SCF) and geometry convergence criteria were employed, and structures were optimized in the gas phase without the use of symmetry constraints. Harmonic frequency analysis based on analytical second derivatives was used to characterize the optimized geometries as local minima.

Acid Stability of Nonradioactive Metal Complexes. A sample of 1 mg of the copper complex was dissolved in 1 mL (affording a $\sim 2 \times 10^{-3}$ M solution). A portion of 1 mL of 10 M HCl was added, and the absorption spectrum (400−900 nm) of the corresponding solution was measured immediately (t_0). The solution was then incubated in an oil bath at 90 °C. The absorption spectrum was remeasured at different time points, and data were fitted with a first-order dissociation kinetics model ($[A] = [A]_0 e^{-kt}$) to estimate the half-life using the Igor Pro software package.

Radioactive Copper Complexes. The general procedure was as follows: $^{64}CuCl_2$ (0.1−0.4 mCi, in 30 μL, purchased from University of Wisconsin—Madison) was diluted with 270 μL of pH 8 sodium citrate (10 mM). A sample of 10 μL of a 0.1 mM ligand solution (in HEPES pH 7.4) was added (affording a final ligand concentration of <0.01 mM), and the reaction mixture was heated at 70 °C for 15 min. Subsequent reaction monitoring was done by analytical HPLC, method D. Under these conditions, all pycup derivatives form the desired radiochemical complex with quantitative yields. These crude radiochemical reaction mixtures were stable over at least 48 h (evaluated by HPLC); no decomplexation or loss of copper is observed. Observed retention times: ^{64}Cu(DOTA): 4.8 min; [Cu(pycup2A)]: 6.6 min; $[Cu(pycup1A1Bn)]^+$: 8.8 min; $[Cu(pycup2Bn)]^{2+}$: 8.9 min; free ^{64}Cu in serum: 4.2 min.

Excess Ligand Challenge Experiment. A 100 μL aliquot of the radiolabeled ligand or peptide conjugate (ligand concentration <0.01 mM) was added to 100 μL of DOTA (1 mM, HEPES buffer, pH 7.4), affording a solution with over 100-fold excess DOTA. The solution was then incubated for 24 h at 37 °C or for 48 h at 70 °C. The 10 μL aliquots were removed at specific time points and analyzed for transchelation using HPLC, method D.

Rat Plasma Stability. A 100 μL aliquot of the radiolabeled ligand or peptide conjugate (ligand concentration <0.01 mM) was added to 400 μL of rat plasma (Lampire Biological Laboratories). The solution was then incubated for 24 h at 37 °C. The 100 μL aliquots were removed at specific time points, diluted with 200 μL HEPES buffer, and filtered using a 0.2 μm filter. A 100 μL aliquot of this filtrate was analyzed for transchelation using HPLC, method D.

Animal Models. All experiments were performed as previously published, in accordance with the NIH Guide for the Care and Use of Laboratory Animals, and were approved by the Massachusetts General Hospital Subcommittee on Research Animal Care.

Biodistribution of [^{64}Cu(pycup2A)]. Three BALB/c mice were injected with ∼5 μCi of radiochemically pure [^{64}Cu-(pycup2A)] through a tail vein catheter. The animals then were sacrificed 2 h post injection, and organs were harvested and weighed; their corresponding activity was counted using a Packard, CobraII Auto gamma scintillation well counter. The radioactivity in each tissue was reported as percent-injected dose per gram (%ID/g), which was calculated by dividing the counts of ^{64}Cu per gram of tissue by the total counts of the injected dose.

PET-CT and Biodistribution of FBP12. Four male Wistar rats (350−400 g) were anesthetized with isoflurane (1−2% in 70% N_2O and 30% O_2), and the body temperature was kept at 37.5 °C. The right femoral vein was cannulated for probe injection. The right femoral artery was cannulated for blood sampling. An incision was made in the neck, and the right common carotid artery was isolated. Intramural thrombus was produced by crushing the right common carotid artery with hemostat clamps for 5 min. Probes were injected within 20 min of thrombus formation. The rat was then placed in a cradle and positioned in a Gamma Medica Triumph Micro PET/CT/SPECT. Each rat was injected with approximately 0.3−0.4 mL and 300−500 μCi of the dose solution, and the animal underwent a 90 min dynamic PET scan with the field of view centered on the neck. The total activity injected was calculated by subtracting the activity in the syringe before injection from the activity remaining in the syringe after injection as measured on a dose calibrator (Capintec CRC-25PET). After the PET imaging, a CT image of the same anatomical region was obtained. The CT scan was performed with a continuous infusion of CT contrast (Isovue, Bracco Diagnostics Inc., Princeton NJ, USA infused at 0.3 mL/min) to delineate the major blood vessels.

During the imaging study serial blood draws were collected from the femoral artery at 0, 2, 5, 10, 15, 30, 60, and 120 min postinjection into EDTA blood tubes. Blood was weighed, and radioactivity in the blood was measured on a gamma counter (Packard, CobraII Auto gamma) to assess clearance of total ^{64}Cu. Animals were euthanized two hours post injection, and the organ distribution of ^{64}Cu was quantified *ex vivo*. The thrombus (located in the right carotid artery), the contralateral carotid artery, blood, urine, intra-abdominal organs, brain, left rectus femoris muscle, and left femur bone were collected from all animals. The tissues were weighed, and radioactivity in each tissue was measured on a gamma counter, along with a weighed aliquot of the injected dose solution. The radioactivity in each tissue was reported as percent-injected dose per gram (%ID/g). The right and left carotid arteries were further analyzed by autoradiography using a multipurpose film and a Perkin-Elmer Cyclone Plus Storage Phosphor system. Data were analyzed by using the Student's *t*-test where *P*-values of less than 0.05 were considered statistically significant. Uncertainties are expressed as the standard error of the mean.

PET Image Analysis. The PET data were dynamically reconstructed with varying time windows. The volume of interest (VOI) analysis of the reconstructed and coregistered PET and CT data was performed with Amide.[40] The CT image was used as guidance to identify the VOI regions. VOI of carotid arteries were determined guided by contrast agent present in the blood vessel and the region of high activity from the PET image (from the thrombus). The contralateral artery VOI was chosen to be the same size as the VOI derived for the thrombus in the ipsilateral artery.

RESULTS AND DISCUSSION

Preparation of Ligands and Complexation with Cu(II). All intermediates and final products were characterized by using ^{1}H, ^{13}C NMR spectroscopy; the connectivity was confirmed using proton−proton and proton−carbon correlation 2D NMR (HSQC and HMBC). The synthesis of pycup derivatives differs considerably from the synthesis of other cross-bridged systems.[41] Unlike most alternative caged or cross-bridged

Scheme 1. Synthesis Scheme of Model Ligand Systems Synthesized[a]

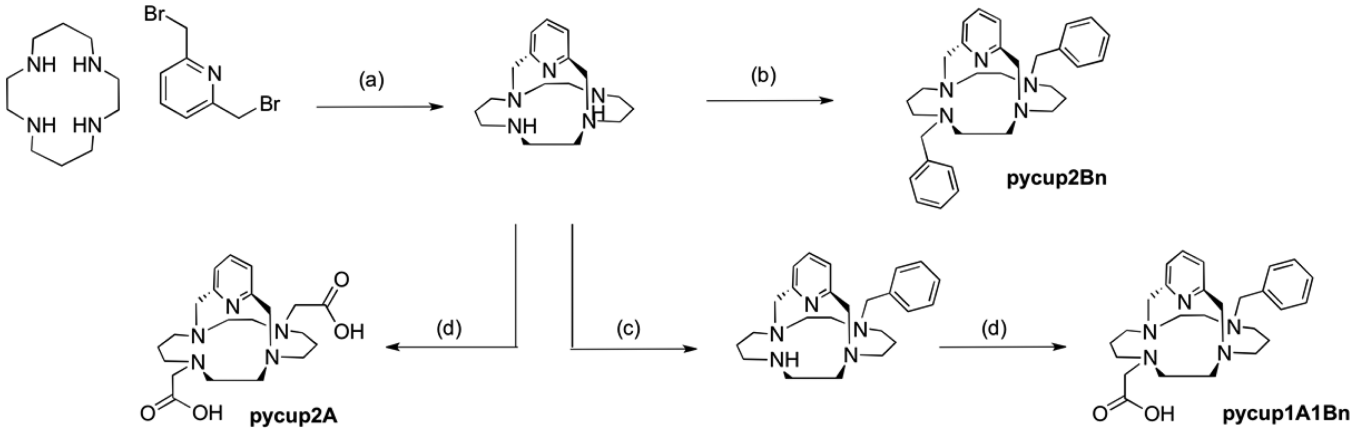

[a](a) $CHCl_3$, Na_2CO_3, rt, 24 h. (b) Benzyl bromide (2.5 equiv), MeCN, rt, 18 h. (c) benzyl bromide (0.65 equiv), MeCN, rt, 18 h. (d) (i) *tert*-butylbromoacetate (1.5 equiv), 50 C, 24 h. (ii) DCM/TFA (1:1), rt, 16 h.

systems, synthesis of pycup is facile and does not require metal-templating or multistep protecting group chemistries. Instead, the pycup ligand can be furnished in one step using intramolecular cross-bridging using 2,6-bis(bromomethyl)-pyridine.[22]

A low yield of only 14% for intramolecular cyclization was obtained which is likely due to competing intermolecular reactions that were observed even under high dilution conditions. Importantly, the corresponding cyclen analogue cannot be formed under the same reaction conditions. Single or double alkylated products such as pycup2A^{t}Bu and pycup2Bn can be synthesized under standard conditions using 0.5−2.5 equiv of alkyl bromide (*tert*-butyl-bromoacetate or benzyl bromide) as an electrophile in the presence of inorganic base (K_2CO_3). The low solubility of the pycup scaffold in acetonitrile was alleviated by the addition of DMF. Single alkylated products were separated from the double-alkylated products by preparative HPLC using a neutral mobile phase and gradient method. In the case of pycup1A^{t}Bu1Bn, pycup1Bn was alkylated under the same conditions as above, but with the addition of KI and heating in order to increase the efficiency of the second, less favored alkylation. The pycup1A^{t}Bu1Bn product was isolated using preparative HPLC as described above. In the case of pycup2A^{t}Bu and pycup1A^{t}Bu1Bn, the *tert*-butyl protection group was removed using a 1:1 mixture of DCM and TFA overnight. All derivatives were synthesized within a maximum of four easily reproducible steps (Scheme 1).

Subsequent complexation of the ligands with $Cu(ClO_4)_2 \cdot 6H_2O$ at pH 5−6 (adjusted using 0.1 M NaOH or HCl) provided the corresponding copper complexes as confirmed by LC-MS. Immediate complex formation occurs upon adjustment of the pH as was evident from the color change of the solution from light blue ($[Cu(H_2O)_6]^{2+}$) to a turquoise or dark blue depending on the Cu complex environment. Purification of Cu complexes was achieved using reverse-phase chromatography with C18 sep-pak cartridges where the separation was monitored by observation of the color change of the eluate from light blue (uncomplexed copper) to dark blue or turquoise (copper complex). The complexes were loaded onto the prerinsed cartridge in H_2O and eluted using a 1:1 mixture of H_2O/EtOH. Fractions containing the complexes were analyzed using LC-MS. The solvent was evaporated to afford the complexes as turquoise or blue microcrystalline powders.

Solid State Crystal Structure of $[Cu(pycup2Bn)]^{2+}$. Crystals suitable of X-ray diffraction were obtained by dissolution of the $[Cu(pycup2Bn)]^{2+}$ complex in 5 M HCl and heating at 60 °C. The single-crystal X-ray structure of the macrocyclic complex revealed well-defined sheets of macrocyclic cations separated by layers filled with disordered solvent molecules (which were not individually modeled, but rather collectively taken into account using the SQUEEZE module of Platon) and chloride counterions; the overall stoichiometry (3Cl:Cu) suggests a singly protonated species must be present in the solvent. Relevant bond lengths and angles are provided in Table 1; the molecular structure is shown in Figure 3.

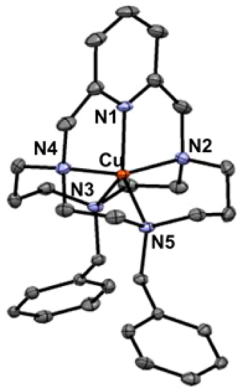

Figure 3. Molecular structure of the cation $[Cu(pycup2Bn)]^{2+}$ (thermal ellipsoids are drawn at 50% probability level). Hydrogen atoms, counterions, and solvent molecules are omitted for clarity.

The coordination geometry of copper is typical of copper(II) complexes with a N-donor polydentate ligand: the metal is five-coordinate, all five nitrogen donors of the macrocycle are bound to the central copper cation, and no additional solvent or anion is present within the bonding distance of the metal. Copper−nitrogen bond lengths range from 1.954(3) Å (Cu−N1) to 2.154(2) Å (Cu−N5); these distances are common for coordination bonds formed by copper(II) and neutral nitrogen donors.[6] The shortest Cu−N contact is between the copper center and the pyridine nitrogen (N1), followed by the contact

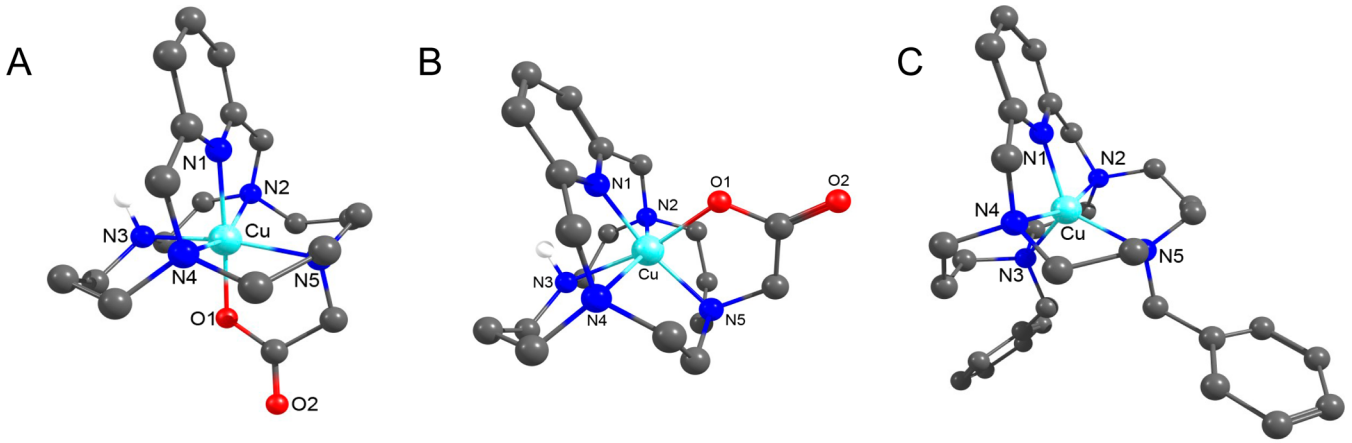

Figure 4. DFT optimized structures of (A) *trans*-[Cu(pycup1A1H)]$^{+}$, (B) *cis*-[Cu(pycup1A1H)]$^{+}$, and (C) [Cu(pycup2Bn)]$^{2+}$. Selected atoms have been numbered, and hydrogen atoms bonded to carbon have been omitted for clarity. Gray = carbon; blue = nitrogen, cyan = copper; red = oxygen; white = hydrogen.

Table 1. Comparison of the Various Geometric Parameters between the Experimental X-ray Single Crystal Structure and DFT Optimized Structure of the [Cu(pycup2Bn)]$^{2+}$ Complex and Selected Optimized Structural Parameters for the Two Geometric Isomers of [Cu(pycup1A1H)]$^{+}$

parameters [*r*: Å; *a*: deg]	X-ray structure	DFT structure [Cu(pycup2Bn)]$^{2+}$	DFT structure *trans*-[Cu(pycup1A1H)]$^{+}$	DFT structure *cis*-[Cu(pycup1A1H)]$^{+}$
r(Cu−N1)	1.953	2.003	2.113	1.921
r(Cu−N2)	2.053	2.115	2.362	2.258
r(Cu−N3)	2.154	2.208	2.060	2.420
r(Cu−N4)	2.053	2.115	2.314	2.312
r(Cu−N5)	2.154	2.208	2.102	2.011
r(Cu−O1)			1.970	2.037
a(N1−Cu−N2)	81.0	80.9	76.3	83.0
a(N1−Cu−N3)	124.8	124.0	92.0	85.1
a(N2−Cu−N3)	87.4	86.8	82.5	74.1
a(N2−Cu−N4)	161.9	161.8	154.7	155.5
a(N3−Cu−N5)	110.3	112.1	169.4	108.4
a(N1−Cu−N5)	124.8	124.0	98.3	165.4
a(N1−Cu−O1)			176.9	83.5
a(N2−Cu−O1)			106.1	100.8
a(N3−Cu−O1)			86.4	168.0
a(N4−Cu−O1)			99.1	97.9
a(N5−Cu−O1)			83.4	83.3
RMSD/Å[a]		0.1164		

[a]NB: The mass weighted RMSD value was calculated based on the atomic positions of all heavy atoms. The two benzyl groups showed significant distortion in the experimental structure. For these atoms, one ring position was selected and used as an input geometry and subsequently for comparison with the DFT optimized structure.

with the adjacent tertiary amines of the pyridine bridge (N2, N4); the longest contacts are with the benzylated cyclam nitrogens (N3, N5); this is consistent with the relative ligand field strength of these nitrogen donors and the overall conformation of the bridged cyclam. The coordination geometry of copper in the pyridine-bridged cyclam is nearly trigonal, with the trigonal plane formed by the pyridine nitrogen (N1) and two tertiary amines from the benzylated fragment of cyclam (N3, N4) and the tertiary amine bridgehead nitrogens (N2, N4) occupying apical positions (with the corresponding bond angle, N2−Cu−N4, 161.90(15)°. The trigonal distortion parameter τ, which ranges from 1 for ideal trigonal bipyramidal geometry to 0 for ideal tetragonal pyramid,[42] is 0.86 for the macrocyclic cation described herein. The cyclam macrocyclic ring is folded, although both six-membered chelate rings adopt chair conformations. This represents a stark contrast to the structures reported of the strapped bis-amide complexes by Hegedus and coworkers.[28] In that case, the six-membered metallacycles cannot fold into chair conformation due to the sp^2-hybridization of the two amide-carbons, which subsequently leads to copper adopting octahedral coordination with an ethyl acetate coordinated as an additional, monodentate ligand.

Computational Study of [Cu(pycup2Bn)]$^{+2}$ and [Cu-(pycup1A1H)]$^{+}$. As we were only able to obtain single crystals suitable for X-ray diffraction for the [Cu(pycup2Bn)]$^{2+}$ complex, we employed density functional theory (DFT; B3LYP/LANL2DZ) calculations to investigate the optimized Cu(II) coordination environment when chelated by pycup derivatives with acetate groups available for coordination. The DFT optimized structure of [Cu(pycup2Bn)]$^{2+}$ was compared to that of the experimental single crystal X-ray structure (Figure 4 and Table 1).

The comparison of the experimental and DFT calculated structure of $[Cu(pycup2Bn)]^{2+}$ revealed a weighted root-mean-squared-displacement (RMSD) between all heavy atoms (C, N, and Cu) of only 0.1164 Å. All other bond lengths and angles lie within standard errors for DFT calculations with the largest deviation in bond length of only 0.062 Å for the r(Cu−N2) and r(Cu−N4) bonds.

The small RMSD value between the calculated and the experimental structures confirms that the calculations faithfully reproduce the geometric structure of this class of complexes and provides confidence in our subsequent analysis of the computational data.

The DFT optimized geometric isomers of $[Cu(pycup1A1H)]^{+}$ revealed that, in the gas phase, the trans isomer is more stable than the cis isomer with a standard free energy difference of ΔG(trans−cis) = −83 kJ mol^{-1}. This energy difference is enthalpic in nature with ΔH(trans−cis) = −85 kJ mol^{-1}. Examination of the structures reveals that both geometric isomers of Cu(pycup1A1H) are highly distorted with asymmetry observed in the Cu−N bond lengths (Table 1). For example, in *trans*-$[Cu(pycup1A1H)]^{+}$ the N2 and N4 atoms are both cis to the pyridine N1 atom yet the Cu−N2 and Cu−N4 bond lengths are 2.362 Å and 2.311 Å, respectively. A similar trend is observed in the geometry of the *cis*-$[Cu(pycup1A1H)]^{+}$ isomer. The calculations predict that, in the *trans*-$[Cu(pycup1A1H)]^{+}$ isomer, a strong Jahn−Teller distortion is observed across the macrocyclic ring involving the two bridge-head nitrogen atoms N2 and N4.

Acid Stability. For suitable cross comparison with previously investigated systems from literature, we subjected the three model complexes to acid-mediated decomplexation under strongly forcing conditions. Dissolution of the copper complex in 5 M HCl and followed by measurement of the UV−vis spectrum (Figure S4) between 400 and 900 nm provided the t = 0 data points, as we had previously found that all three complexes exhibited very slow decomplexation at room temperature. The acidic solution was then heated at 90 °C, and samples were removed at specific time points and monitored by UV−vis spectroscopy.

Under these conditions, we observed a half-life of 2.7 h for dissociation of copper from the complex with pycup2A and 1.5 h for dissociation of copper from pycup1A1Bn. The copper complex of pycup2Bn proved to be much more kinetically inert with a half-life of 20.3 h.

All Cu(pycup) derivatives were found to be more stable to decomplexation than the DOTA (reproduced as a control) and NOTA (from ref 3) complexes. The Cu(pycup) derivatives were inferior to, but more comparable with, the highly inert complexes [Cu(CB-TE2A)] and $[Cu(SarAr)]^{2+}$ (Table 2). Our results are comparable to what Denat and co-workers obtained for DO2A type derivatives with an ether crossbridge.[21] We hypothesize that the protonation of the acetate arm(s) results in initial aquation of the copper complexes of pycup2A and pycup1A1Bn, and this results in eventual dissociation of the metal ion. Collectively, these data indicated that integration of the pyridyl ligand moiety into the cross-bridge was advantageous for increased kinetic inertness.

Radiolabeling. Radiolabeling conditions for ^{64}Cu can range from a pH of 5 to above 7, depending on the ligand used. We observed radiolabeling yielding only up to 20% product under conditions below pH 7 for all pycup derivatives, which prompted us to use more basic conditions above pH 7. Due to the proton-sponge nature of the pycup ligand,[22] deprotonation or exchange of the metal ion with the proton trapped by the ligand at lower pH ranges becomes much more difficult. We preformed the ^{64}Cu(citrate) complex to avoid formation of colloidal $Cu(OH)_2$ at elevated pH and added the ^{64}Cu(citrate) complex to pycup ligand solutions in pH 7.4 HEPES buffer. Ligand concentrations as low as 10 μM were able to provide quantitative yields within 15 min at 70 °C, affording specific activities of 100 mCi/μmol. We observed same radiolabeling conditions for all derivatives synthesized. Lower temperatures such as 60 °C provide quantitative yields within 30 min. We hypothesize that the rigid preorganized structure of pycup is the reason for the need to label at increased temperatures. The cross-bridged structure can likely not invert as readily as more flexible ligand systems such as triethylenetetramine (TETA) or DOTA. Figure 5 shows crude radiolabeling traces obtained using the conditions described above. Nevertheless, the radiolabeling conditions require shorter reaction time at a lower temperature as CB-TE2A conjugates.

Table 2. Half-Lives for the Dissociation of Cu(II) Complexes in 5 M HCl and 90 °C[a]

ligand	$t_{1/2}$
pycup2A	2.7 h
pycup1A1Bn	1.5 h
pycup2Bn	20.3 h
DOTA	<3 min
NOTA	<3 min[3]
CB-TE2A	156 h[3]
SarAr	∼40 h[3]
C3B-TE2A	*b*
[Cu(L1)]	4.3 h

[a]DOTA was measured as a control, values found for previously published ligands NOTA, CB-TE2A, SarAr, C3B-TE2A,[20] and [Cu(L1)].[21] [b]The authors report no decomplexation for up to 7 days.

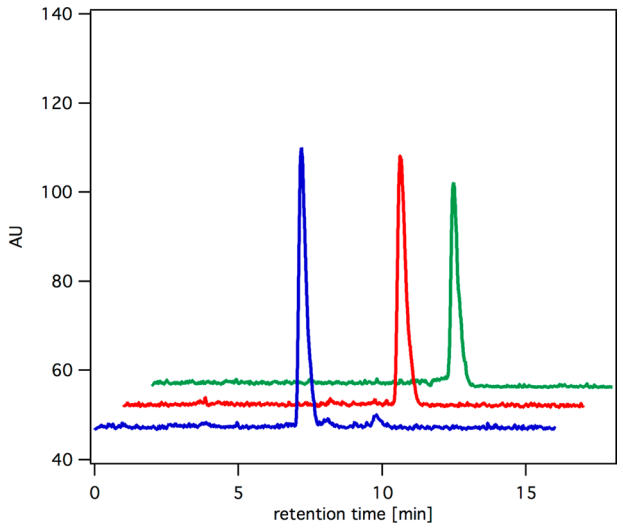

Figure 5. Radio-HPLC traces of the crude reaction mixture after 15 min at 70 °C are shown for the radiochemical complexes $[^{64}Cu(pycup2A)]$ (blue), $[^{64}Cu(pycup1A1Bn)]^{+}$ (red), and $[^{64}Cu(pycup2Bn)]^{2+}$ (green). One-minute offsets of the red and green trace are used for clearer delineation of the product peaks.

DOTA Ligand Challenge and Rat Plasma Challenge of Model Complexes. Table 3 summarizes the percentage transchelation under different conditions at select time points.

Table 3. Summary of Stability Data of Radiochemical ^{64}Cu Complexes of the Investigated Ligand Systems Using Excess DOTA Challenge and Plasma Challenge[a]

challenge experiment	ligand [time point, % complex stability]								
	pycup2A			pycup1A1Bn			pycup2Bn		
	2 h	12 h	24 h	2 h	12 h	24 h	2 h	12 h	24 h
>100 equiv DOTA (37 °C)	95	96	95	99	96	96	99	95	93
	2 h	24 h	48 h	2 h	24 h	48 h	2 h	24 h	48 h
>100 equiv DOTA (70 °C)	97	95	95	98	95	95	97	91	91
	0.5 h	12 h	24 h	0.5 h	12 h	24 h	0.5 h	12 h	24 h
rat plasma (37 °C)	98	98	98	99	99	98	97	98	97

[a]Data are provided as % intact radiochemical complex at the corresponding time point.

To assess the *in vitro* stability of the formed radiolabeled model complexes, we conducted two different *in vitro* challenge experiments. We first used over 100 equiv of DOTA to assess transchelation with a potent copper chelator (log K for $[Cu(DOTA)]^{2-}$ = 22.2)[3] at 37 °C in pH 7.4. We found that within 24 h, all complexes were stable with <7% decomplexation observed (Table 3). To determine the thermodynamic equilibrium state of this transchelation reaction, we also conducted the same experiment at 70 °C, over a time frame of 48 h. We observed a maximum transchelation to DOTA of ≤9% which persisted after 15 h incubation demonstrating that all ^{64}Cu(pycup) complexes investigated are at least an order of magnitude more thermodynamically stable than $[Cu(DOTA]^{2-}$ at pH 7.4.

As a second challenge experiment, we incubated the radiolabeled complexes in rat plasma at 37 °C and quantified the percentage of intact radiochemical complex at 30 min, 1 h, and 24 h. We found that the model complexes were all highly stable under these conditions even after 24 h (≥97% intact).

Biodistribution of [^{64}Cu(pycup2A)]. We next evaluated the biodistribution of a nonderivatized pycup derivative. We radiolabeled pycup2A, using conditions described above. Balb/c mice (n = 3) were injected with equivalent radioactive doses of [^{64}Cu(pycup2A)], sacrificed, and organs harvested 2 h post injection. Biodistribution studies revealed only background levels of activity were retained in the animals at 2 h p.i. Importantly, liver accumulation of radioactivity was very low (1.14 ± 0.21%ID/g) providing additional confirmation of the stability of our Cu-complexes *in vivo*.[6]

We observed low levels of activity in the kidneys (2.05 ± 0.19%ID/g) and very high levels of radioactivity in the urine, consistent with rapid renal clearance. Almost all of the activity cleared the animals by 2 h. The biodistribution of [^{64}Cu-(pycup2A)] shows a favorable clearance profile and low uptake in nontarget organs, which provides a firm basis for the development of targeted agents using the pycup technology (Table 4).

Bioconjugation. To demonstrate that our new ligand system can be easily conjugated to biomolecules, we linked pycup2A to a fibrin-binding specific peptide via amide bond formation with a carboxylate of pycup2A. The fibrin-binding peptide originated from a phage display screen by Kolodzjej et al.[43] and has been used in other fibrin targeted imaging probes.[34,44] Fibrin is a principal component of blood clots[45] and represents a suitable imaging target for the detection of thrombus (blood clot). Thrombus is implicated in devastating cardiovascular diseases such as stroke, myocardial infarction, and deep-vein thrombosis.

The fibrin-binding peptide, with two terminal amine functional groups, was dissolved in a minimal amount of DMF and added to the PyBOP activated ligand pycup2A. The pH was adjusted to 7, and the reaction mixture was allowed to stir overnight. The excess pycup2A provided essentially exclusive formation of the desired, diamidated product. We observed that product only formed when the pH was maintained at 7 or slightly below, likely due to partial protonation of the terminal amines of the peptide under more acidic conditions. Purification of the peptide using preparative HPLC, and an acidic mobile phase provided the desired product in moderate yields. Successful conjugate (structure shown in Figure 6) was confirmed by detection of the $[M + 2H]^{2+}$ ion using LC-MS. Formation of the corresponding copper complex was performed using the same method as described in the Experimental Section for the model complexes.

Table 4. Biodistribution Data for [^{64}Cu(pycup2A)] in Balb/c Mice (n = 3) at 2 h Post-Injection Expressed as Percent Injected Dose per Gram of Organ (%ID/g)

organ/tissue	average (% ID/g, ±std. dev.)
blood	0.04 ± 0.01
liver	1.14 ± 0.20
heart	0.05 ± 0.01
lung	0.21 ± 0.01
spleen	0.12 ± 0.04
intestine	0.32 ± 0.07
kidney	2.05 ± 0.19

Thrombus Imaging Using FBP12. We have been interested in fibrin targeting for some time[34,46,47] and recently characterized several fibrin-targeted peptides conjugated with DOTA-monoamide and labeled with ^{64}Cu for thrombus PET imaging.[34] In that study, we found that the ^{64}Cu(DOTA-monoamide)-labeled peptide (termed FBP2 and analogous to the structure in Figure 6) showed good thrombus uptake in a rat model of acute arterial thrombosis, and that the thrombi were readily apparent in PET images. We also found however, that FBP2 was not fully stable *in vivo* and there was some transmetalation of ^{64}Cu from the probe to plasma proteins. This transmetalation resulted in higher blood background and limited the thrombus:background levels that could be achieved. Here, we tested the hypothesis that a more inert copper chelate should result in greater thrombus:background levels. We evaluated the ^{64}Cu-labeled bioconjugate FBP12 using the same crush injury model of carotid artery thrombosis as used previously.[34]

PET images with the pycup derivative FBP12 clearly delineate the thrombus in the right carotid artery. Figure 5 shows three orthogonal PET images taken through the region of high activity denoted by the yellow arrow. CT angiography

dx.doi.org/10.1021/mp400686z | Mol. Pharmaceutics 2014, 11, 617−629

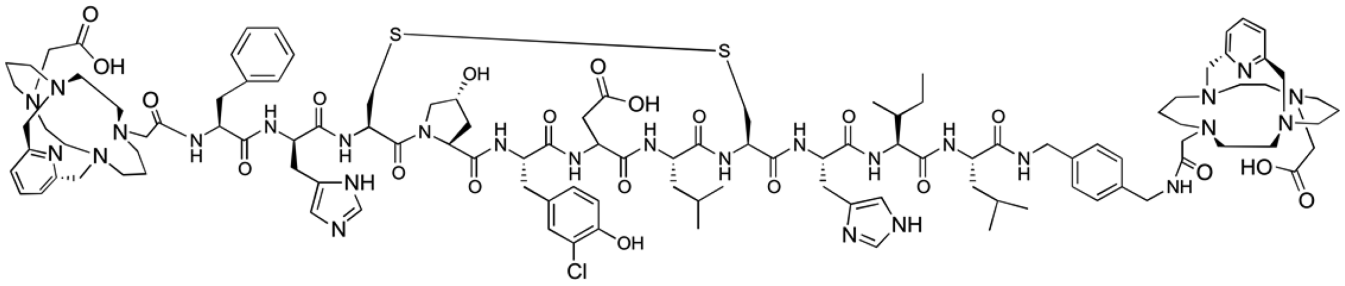

Figure 6. Chemical structure of the pep(12) conjugate.

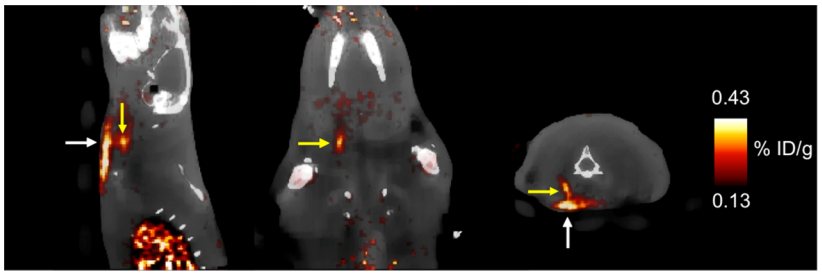

Figure 7. Fused PET/CT sagittal (left), coronal (middle), and transaxial (right) images (30–90 min p.i.) of a rat with a carotid artery thrombus using FBP12. The yellow arrow denotes the location of the engineered clot with high activity; the white arrow indicates the surgical incision site which also shows high activity due to microthrombi.

confirmed that this region of high activity was localized to the right common carotid artery, the site at which the thrombus was induced. This model also results in some microthrombosis around the surgical site.[34,48] Figure 7 shows that the surgical site is strongly enhanced by FBP12 (white arrows). It is apparent from the sagittal (left) and axial (right) images that the enhancement of the surgical site is superficial (white arrow), while the carotid thrombus is deeper in the neck (yellow arrow). The coronal (middle) and axial (right) images also demonstrate that there is very little activity in the contralateral artery.

The images were quantitatively analyzed by taking a volume of interest (VOI) that covered the focal activity in the right carotid and comparing it to the same sized VOI in the left carotid. Time activity curves (Figure S7, Supporting Information) showed increased initial activity in both vessels after injection, but the signal in the left carotid clears rapidly while signal clears more slowly from the right carotid. The ratio of right carotid–left carotid VOI was 2.96 ± 0.42 at 90 min post injection. We also analyzed the carotid artery segments *ex vivo* using autoradiography (Figure S8, Supporting Information). Autoradiography confirmed higher activity in the clot containing vessel, and the ratio of activity (right carotid–left carotid) in the autoradiography images was 1.5 ± 0.19. *Ex vivo* biodistribution data (Table 5) showed higher activity in the thrombus than in the blood, brain, heart, muscle, bone, and contralateral artery. At 2 h post injection, most of the activity had cleared the animal.

Although clear delineation the thrombus in the right carotid artery (Figure 7) as well as the microthrombi induced through injury at the surgical site was possible, the quantitative analysis showed that pycup derivatized FBP12 showed similar efficacy to the DOTA conjugate FBP2 reported previously. It was anticipated that the greater kinetic inertness conferred by the pycup chelator compared to DOTA-monoamide would result in less transchelation of ^{64}Cu to plasma proteins and reduced background.

Table 5. Biodistribution and Clot-to-Organ Ratios of Probe FBP12 in a Rat Model of Arterial Thrombus at 2 h Post-Injection (n = 4)

organ/tissue	average (% ID/g, ± std. dev.)	clot:organ ratio, ± std. dev.
clot	0.38 ± 0.08	1.00 ± 0.00
contra	0.23 ± 0.04	1.67 ± 0.21
muscle	0.09 ± 0.07	6.63 ± 1.59
bone	0.07 ± 0.01	5.39 ± 0.65
brain	0.01 ± 0.00	42.48 ± 4.90
blood	0.09 ± 0.01	4.31 ± 0.65
heart	0.11 ± 0.04	4.24 ± 0.92
intestine	0.38 ± 0.11	1.14 ± 0.26
lungs	0.64 ± 0.32	0.83 ± 0.19
spleen	0.50 ± 0.07	0.76 ± 0.04
liver	2.53 ± 0.09	0.15 ± 0.02
kidney	2.75 ± 0.05	0.14 ± 0.02

As expected, we observed about half the activity in the blood at 2 h for FBP12 vs FBP2 (0.09 ± 0.01 vs 0.164 ± 0.016, respectively). However, we also saw less uptake in the thrombus for FBP12, and this limited the overall efficacy. An analysis of blood sampled at different times post injection indicated that the probe FBP12 underwent rapid metabolism, and this also limited overall efficacy. A functional assay was used to determine the fraction of active fibrin binding probe present (Figure S5). We also performed HPLC analysis of the plasma (Figure S6). Both analyses showed that only 50% of the plasma activity at 15 min post injection was intact probe.

We then looked at the stability of radiolabeled FBP12 incubated with plasma (Figure S3). This *in vitro* assay clearly showed that the complex underwent significant degradation in plasma after 30–60 min. Because the model compounds were stable in plasma, the plasma instability of FBP12 can be traced to degradation of the peptide and not release of ^{64}Cu. Comparison of the HPLC traces of FBP12 in plasma with plasma samples spiked with $^{64}CuCl_2$ confirmed that the

dx.doi.org/10.1021/mp400686z | *Mol. Pharmaceutics* 2014, 11, 617–629

decomposition products were not equivalent to plasma protein-bound copper.

Future work will address the root of this peptide instability and focus on medicinal chemistry approaches to prepare more metabolically robust peptides.

The pycup ligand and its bifunctional derivatives represent a new class of chelators for ^{64}Cu. While we have prepared derivatives with pendant carboxylates and successfully conjugated one of these to a peptide, it is apparent that other conjugation strategies can be employed. The stability data with $[Cu(pycup2Bn)]^{2+}$ suggest that the pentadentate pycup ligand itself is sufficient for robust labeling and formation of an inert complex with copper. This allows one or both of the secondary amines on pycup to be modified with a functional group for bioconjugation and/or chemical modification to alter overall charge or lipophilicity. The ease of synthesis of pycup and its derivatives, including differentiation of one of the secondary amines, results in tremendous flexibility in using pycup derivatives to not only chelate ^{64}Cu but also to modify the pharmacokinetic properties of the conjugate. Because derivatization with a mixture of donor arms is easily attainable, the pycup ligand could be linked easily to multiple targeting moieties simultaneously, using bioorthogonal functional group chemistry. The possibility for asymmetric derivatization of the two secondary nitrogens also opens up additional possibilities for the development of trifunctional derivatives. Such an approach could establish pycup as a convenient chelator and conjugation tool for multimodal systems. These research endeavors as well as conjugation of pycup to other peptides are ongoing.

CONCLUSION

In conclusion, we successfully developed the cross-bridged bicyclic ligand system pycup for rapid chelation of ^{64}Cu and subsequent formation of a kinetically inert complex. Pycup provides an N_5 ligand donor set, which can be easily modulated by alkylation of the two secondary amines present. The addition of donor groups such as acetates does not impact the radiolabeling properties of the ligand or the thermodynamic and kinetic inertness of the corresponding copper complexes significantly. Conjugation to a target-specific peptide and subsequent PET imaging *in vivo* is easily attainable, as exemplified by the conjugation to a fibrin-binding peptide for the imaging of thrombus in rats. The flexible and facile functionalization of the ligand pycup provides future opportunities for conjugation to more than one targeting vector. Pycup is well-suited for conjugation to other commonly used targeting vectors, providing radiochemists with a new mean for visualization of biomolecules using ^{64}Cu.

ASSOCIATED CONTENT

Supporting Information

Radio-HPLC traces of competition studies, UV−vis absorption spectra, experimental details and results of the functional fibrin binding assay, plasma and blood stability of FBP12, VOI analysis, and *ex vivo* autoradiography. This material is available free of charge via the Internet at http://pubs.acs.org.

AUTHOR INFORMATION

Corresponding Authors

*E-mail: eboros@nmr.mgh.harvard.edu.

*E-mail: caravan@nmr.mgh.harvard.edu.

Notes

The authors declare the following competing financial interest(s): P.C. has equity in Factor 1A, LLC, the company which holds the patent rights to the peptides used in these probes.

ACKNOWLEDGMENTS

Dr. Peter Mueller (X-ray diffraction facility, MIT chemistry department) is warmly acknowledged for assistance with elucidation of the solid state crystal structure of $[Cu(pycup2Bn)]^{2+}$. P.C. acknowledges the National Heart, Lung, and Blood Institute for funding (NHLBI, award HL109448) and an instrumentation grant from the National Center for Research Resources (NCRR, award RR029495) for the micro-PET/SPECT/CT. E.B. and J.P.H. thank the Swiss National Science Foundation and the Australian National Science and Technology Organization for support, respectively. E.R.A. acknowledges the US Department of Energy Office of Basic Energy Science. The X-ray diffractometer at Tufts was funded by the NSF (MRI: CHE-1229426).

REFERENCES

(1) Holland, J.; Williamson, M.; Lewis, J. Unconventional nuclides for radiopharmaceuticals. *Mol. Imaging* **2010**, *9*, 1−20.

(2) Wadas, T. J.; Wong, E. H.; Weisman, G. R.; Anderson, C. J. Copper Chelation Chemistry and its Role in Copper Radiopharmaceuticals. *Curr. Pharm. Des.* **2007**, *13*, 3−16.

(3) Wadas, T. J.; Wong, E. H.; Weisman, G. R.; Anderson, C. J. Coordinating Radiometals of Copper, Gallium, Indium, Yttrium, and Zirconium for PET and SPECT Imaging of Disease. *Chem. Rev.* **2010**, *110*, 2858−2902.

(4) Copper 64-ATSM and PET/CT Scan in Predicting Disease Progression in Patients With Newly-Diagnosed Stage IB, Stage II, Stage III, or Stage IVA Cervical Cancer Who Are Undergoing Radiation Therapy and Cisplatin Treatment. http://clinicaltrials.gov/show/NCT00794339 (accessed July 5, 2013).

(5) Boros, E.; Cawthray, J. F.; Ferreira, C. L.; Patrick, B. O.; Adam, M. J.; Orvig, C. Evaluation of the H_2dedpa Scaffold and its cRGDyK Conjugates for Labeling with ^{64}Cu. *Inorg. Chem.* **2012**, *51*, 6279−6284.

(6) Boswell, C. A.; Sun, X.; Niu, W.; Weisman, G. R.; Wong, E. H.; Rheingold, A. L.; Anderson, C. J. Comparative in Vivo Stability of Copper-64-Labeled Cross-Bridged and Conventional Tetraazamacrocyclic Complexes. *J. Med. Chem.* **2004**, *47*, 1465−1474.

(7) Bailey, G. A.; Price, E. W.; Zeglis, B. M.; Ferreira, C. L.; Boros, E.; Lacasse, M. J.; Patrick, B. O.; Lewis, J. S.; Adam, M. J.; Orvig, C. H_2azapa: a Versatile Acyclic Multifunctional Chelator for ^{67}Ga, ^{64}Cu, ^{111}In, and ^{177}Lu. *Inorg. Chem.* **2012**, *51*, 12575−12589.

(8) Sibbons, K. F.; Shastri, K.; Watkinson, M. The application of manganese complexes of ligands derived from 1,4,7-triazacyclononane in oxidative catalysis. *Dalton Trans.* **2006**, *5*, 645−661.

(9) Maheshwari, V.; Dearling, J. L. J.; Treves, S. T.; Packard, A. B. Measurement of the rate of copper(II) exchange for ^{64}Cu complexes of bifunctional chelators. *Inorg. Chim. Acta* **2012**, *393*, 318−323.

(10) Ma, M. T.; Cooper, M. S.; Paul, R. L.; Shaw, K. P.; Karas, J. A.; Scanlon, D.; White, J. M.; Blower, P. J.; Donnelly, P. S. Macrobicyclic Cage Amine Ligands for Copper Radiopharmaceuticals: A Single Bivalent Cage Amine Containing Two Lys3-bombesin Targeting Peptides. *Inorg. Chem.* **2011**, *50*, 6701−6710.

(11) Cai, H.; Li, Z.; Huang, C.-W.; Shahinian, A. H.; Wang, H.; Park, R.; Conti, P. S. Evaluation of Copper-64 Labeled AmBaSar Conjugated Cyclic RGD Peptide for Improved MicroPET Imaging of Integrin $\alpha_v\beta_3$ Expression. *Bioconjugate Chem.* **2010**, *21*, 1417−1424.

(12) Huang, S.; Joso, R.; Fuchs, A.; Barner, L.; Smith, S. V. Probing Solid−Liquid Interfaces Using Radiotracer Technology: Characterization of Functionalized Microspheres. *Chem. Mater.* **2008**, *20*, 5375−5380.

(13) Wong, E. H.; Weisman, G. R.; Hill, D. C.; Reed, D. P.; Rogers, M. E.; Condon, J. P.; Fagan, M. A.; Calabrese, J. C.; Lam, K.-C.; Guzei, I. A.; Rheingold, A. L. Cross-bridged cyclams and pendant arm derivatives. *J. Am. Chem. Soc.* **2000**, *112*, 10561.
(14) Wei, L.; Ye, Y.; Wadas, T. J.; Lewis, J. S.; Welch, M. J.; Achilefu, S.; Anderson, C. J. ^{64}Cu-Labeled CB-TE2A and diamsar-conjugated RGD peptide analogs for targeting angiogenesis: comparison of their biological activity. *Nucl. Med. Biol.* **2009**, *36*, 277−285.
(15) Tircsó, G.; Benyó, E. T.; Suh, E. H.; Jurek, P.; Kiefer, G. E.; Sherry, A. D.; Kovàcs, Z. (S)-5-(p-Nitrobenzyl)-PCTA, a Promising Bifunctional Ligand with Advantageous Metal Ion Complexation Kinetics. *Bioconjugate Chem.* **2009**, *20*, 565−575.
(16) Ait-Mohand, S.; Fournier, P.; Dumulon-Perreault, V.; Kiefer, G. E.; Jurek, P.; Ferreira, C. L.; Bénard, F.; Guérin, B. Evaluation of ^{64}Cu-Labeled Bifunctional Chelate-Bombesin Conjugates. *Bioconjugate Chem.* **2011**, *22*, 1729−1735.
(17) Dumont, R. A.; Deininger, F.; Haubner, R.; Maecke, H. R.; Weber, W. A.; Fani, M. Novel ^{64}Cu- and ^{68}Ga-Labeled RGD Conjugates Show Improved PET Imaging of $\alpha_v\beta_3$ Integrin Expression and Facile Radiosynthesis. *J. Nucl. Med.* **2011**, *52*, 1276−1284.
(18) Altai, M.; Strand, J.; Rosik, D.; Selvaraju, R. K.; Eriksson Karlström, A.; Orlova, A.; Tolmachev, V. Influence of Nuclides and Chelators on Imaging Using Affibody Molecules: Comparative Evaluation of Recombinant Affibody Molecules Site-Specifically Labeled with ^{68}Ga and ^{111}In via Maleimido Derivatives of DOTA and NODAGA. *Bioconjugate Chem.* **2013**, *24*, 1102−1109.
(19) Cooper, M. S.; Ma, M. T.; Sunassee, K.; Shaw, K. P.; Williams, J. D.; Paul, R. L.; Donnelly, P. S.; Blower, P. J. Comparison of ^{64}Cu-Complexing Bifunctional Chelators for Radioimmunoconjugation: Labeling Efficiency, Specific Activity, and in Vitro/in Vivo Stability. *Bioconjugate Chem.* **2012**, *23*, 1029−1039.
(20) Pandya, D. N.; Dale, A. V.; Kim, J. Y.; Lee, H.; Ha, Y. S.; An, G. I.; Yoo, J. New Macrobicyclic Chelator for the Development of Ultrastable ^{64}Cu-Radiolabeled Bioconjugate. *Bioconjugate Chem.* **2012**, *23*, 330−335.
(21) Esteves, C. V.; Lamosa, P.; Delgado, R.; Costa, J.; Désogère, P.; Rousselin, Y.; Goze, C.; Denat, F. Remarkable Inertness of Copper(II) Chelates of Cyclen-Based Macrobicycles with Two trans-N-Acetate Arms. *Inorg. Chem.* **2013**, *52*, 5138−5153.
(22) Brandes, S.; Denat, F.; Lacour, S.; Rabiet, F.; Barbette, F.; Pullumbi, P.; Guilard, R. Synthesis of Macropolycyclic Ligands Based on Tetraazacycloalkanes. *Eur. J. Org. Chem.* **1998**, *11*, 2349−2360.
(23) Roger, M.; Lima, L. M. P.; Frindel, M.; Platas-Iglesias, C.; Gestin, J.-F.; Delgado, R.; Patinec, V.; Tripier, R. Monopicolinate-dipicolyl Derivative of Triazacyclononane for Stable Complexation of Cu^{2+} and $^{64}Cu^{2+}$. *Inorg. Chem.* **2013**, *52*, 5246−5259.
(24) Lima, L. M. P.; Esteban-Gómez, D.; Delgado, R.; Platas-Iglesias, C.; Tripier, R. Monopicolinate Cyclen and Cyclam Derivatives for Stable Copper(II) Complexation. *Inorg. Chem.* **2012**, *51*, 6916−6927.
(25) Gasser, G.; Tjioe, L.; Graham, B.; Belousoff, M. J.; Juran, S.; Walther, M.; Künstler, J.-U.; Bergmann, R.; Stephan, H.; Spiccia, L. Synthesis, Copper(II) Complexation, ^{64}Cu-Labeling, and Bioconjugation of a New Bis(2-pyridylmethyl) Derivative of 1,4,7-Triazacyclononane. *Bioconjugate Chem.* **2008**, *19*, 719−730.
(26) Wynn, T.; Hegedus, L. S. Synthesis and Structural Studies of 1,8-Pyridine-Capped 5,12-Dioxocyclams. *J. Am. Chem. Soc.* **2000**, *122*, 5034−5042.
(27) Achmatowicz, M.; Hegedus, L. S.; David, S. Synthesis and Structural Studies of 5,12-Dioxocyclams Capped by 4-Substituted Pyridines Across the Amine Nitrogens. *J. Org. Chem.* **2003**, *68*, 7661−7666.
(28) Gil, J. M.; David, S.; Reiff, A. L.; Hegedus, L. S. Synthesis and Complexation of "Back-to-Back" Capped Bis-dioxocyclams. *Inorg. Chem.* **2005**, *44*, 5858−5865.
(29) Eisenwiener, K.-P.; Prata, M. I.; Buschmann, I.; Zhang, H.-W.; Santos, A. C.; Wenger, S.; Reubi, J. C.; Mäcke, H. R. NODAGATOC, a New Chelator-Coupled Somatostatin Analogue Labeled with [$^{67/68}$Ga] and [^{111}In] for SPECT, PET and Targeted Therapeutic Applications of Somatostatin Receptor (hsst2) Expressing Tumors. *Bioconjugate Chem.* **2002**, *13*, 530−541.
(30) Krenning, E. P.; Kwekkeboom, D. J.; Bakker, W. H.; Breeman, W. A. P.; Kooij, P. P. M.; Oei, H. Y.; Vanhagen, M.; Postema, P. T. E.; Dejong, M.; Reubi, J. C.; Visser, T. J.; Reijs, A. E. M.; Hofland, L. J.; Koper, J. W.; Lamberts, S. W. J. Somatostatin Receptor Scintigraphy with [In-111-Dtpa-D-Phe(1)]- and [I-123-Tyr(3)]-Octreotide - the Rotterdam Experience with More Than 1000 Patients. *Eur. J. Nucl. Med.* **1993**, *20*, 716−731.
(31) Guo, Y.; Ferdani, R.; Anderson, C. J. Preparation and Biological Evaluation of 64Cu Labeled Tyr3-Octreotate Using a Phosphonic Acid-Based Cross-Bridged Macrocyclic Chelator. *Bioconjugate Chem.* **2012**, *23*, 1470−1477.
(32) Carlucci, G.; Ananias, H. J. K.; Yu, Z.; Hoving, H. D.; Helfrich, W.; Dierckx, R. A. J. O.; Liu, S.; de Jong, I. J.; Elsinga, P. H. Preclinical Evaluation of a Novel ^{111}In-Labeled Bombesin Homodimer for Improved Imaging of GRPR-Positive Prostate Cancer. *Mol. Pharmaceutics* **2013**, *10*, 1716−1724.
(33) Jeong, J. M.; Hong, M. K.; Chang, Y. S.; Lee, Y.-S.; Kim, Y. J.; Cheon, G. J.; Lee, D. S.; Chung, J.-K.; Lee, M. C. Preparation of a Promising Angiogenesis PET Imaging Agent: ^{68}Ga-Labeled c-(RGDyK) Isothiocyanatobenzyl-1,4,7-Triazacyclononane-1,4,7-Triacetic Acid and Feasibility Studies in Mice. *J. Nucl. Med.* **2008**, *49*, 830−836.
(34) Ciesienski, K. L.; Yang, Y.; Ay, I.; Chonde, D. B.; Loving, G. S.; Rietz, T. A.; Catana, C.; Caravan, P. Fibrin-Targeted PET Probes for the Detection of Thrombi. *Mol. Pharmaceutics* **2013**, *10*, 1100−1110.
(35) Sheldrick, G. M. Phase annealing in SHELX-90: direct methods for larger structures. *Acta Crystallogr.* **1990**, *A46*, 467.
(36) Sheldrick, G. M. *SHELXL 97*, Program for Crystal Structure Analysis (Release 97-2); University Göttingen: Göttingen, 1997.
(37) Frisch, M. J.; Trucks, G. W.; Schlegel, H. B.; Scuseria, G. E.; Robb, M. A.; Cheeseman, J. R.; Montgomery, J. A., Jr.; Vreven, T.; Kudin, K. N.; Burant, J. C.; Millam, J. M.; Iyengar, S. S.; Tomasi, J.; Barone, V.; et al. *Gaussian 09*; Gaussian, Inc.: Wallingford, CT, 2009.
(38) Becke, A. Density-functional thermochemistry. III. The role of exact exchange. *J. Chem. Phys.* **1993**, *98*, 5648−5652.
(39) Lee, C.; Yang, W.; Parr, R. Development of the Colle-Salvetti correlation-energy formula into a functional of the electron density. *Phys. Rev. B* **1988**, *37*, 785−789.
(40) Loening, A. M.; Gambhir, S. S. AMIDE: A Free Software Tool for Multimodality Medical Image Analysis. *Mol. Imaging* **2003**, *2*, 131.
(41) Heroux, K. J.; Woodin, K. S.; Tranchemontagne, D. J.; Widger, P. C. B.; Southwick, E.; Wong, E. H.; Weisman, G. R.; Tomellini, S. A.; Wadas, T. J.; Anderson, C. J.; Kassel, S.; Golen, J. A.; Rheingold, A. L. The long and short of it: the influence of N-carboxyethyl versus N-carboxymethyl pendant arms on in vitro and in vivo behavior of copper complexes of cross-bridged tetraamine macrocycles. *Dalton Trans.* **2007**, *21*, 2150−2162.
(42) Addison, A. W.; Rao, T. N.; Reedijk, J.; van Rijn, J.; Verschoor, G. C. Synthesis, structure, and spectroscopic properties of copper(II) compounds containing nitrogen-sulphur donor ligands; the crystal and molecular structure of aqua[1,7-bis(N-methylbenzimidazol-2[prime or minute]-yl)-2,6-dithiaheptane]copper(II) perchlorate. *J. Chem. Soc., Dalton Trans.* **1984**, *7*, 1349−1356.
(43) Kolodziej, A. F.; Nair, S. A.; Graham, P.; McMurry, T. J.; Ladner, R. C.; Wescott, C.; Sexton, D. J.; Caravan, P. Fibrin Specific Peptides Derived by Phage Display: Characterization of Peptides and Conjugates for Imaging. *Bioconjugate Chem.* **2012**, *23*, 548−556.
(44) Botnar, R. M.; Buecker, A.; Wiethoff, A. J.; Parsons, E. C.; Katoh, M.; Katsimaglis, G.; Weisskoff, R. M.; Lauffer, R. B.; Graham, P. B.; Gunther, R. W.; Manning, W. J.; Spuentrup, E. In vivo magnetic resonance imaging of coronary thrombosis using a fibrin-binding molecular magnetic resonance contrast agent. *Circulation* **2004**, *110*, 1463−1466.
(45) Monroe, D. M.; Hoffman, M. What Does It Take to Make the Perfect Clot? *Arterioscler. Thromb. Vasc. Biol.* **2006**, *26*, 41−48.
(46) Overoye-Chan, K.; Koerner, S.; Looby, R.; Kolodziej, A.; Zech, S.; Deng, Q.; Chasse, J.; McMurry, T.; Caravan, P. EP-2104R: a fibrin-

specific gadolinium-Based MRI contrast agent for detection of thrombus. *J. Am. Chem. Soc.* **2008**, *130*, 6025−6039.
(47) Uppal, R.; Ciesienski, K. L.; Chonde, D. B.; Loving, G. S.; Caravan, P. Discrete Bimodal Probes for Thrombus Imaging. *J. Am. Chem. Soc.* **2012**, *134*, 10799−10802.
(48) Uppal, R.; Ay, I.; Dai, G.; Kim, Y.; Sorensen, A.; Caravan, P. Molecular MRI of intracranial thrombus in a rat ischemic stroke model. *Stroke* **2010**, *41*, 1271−1277.